Article

Developmental Cell

Polo Kinase Phosphorylates Miro to Control ER-Mitochondria Contact Sites and Mitochondrial Ca^{2+} Homeostasis in Neural Stem Cell Development

Graphical Abstract

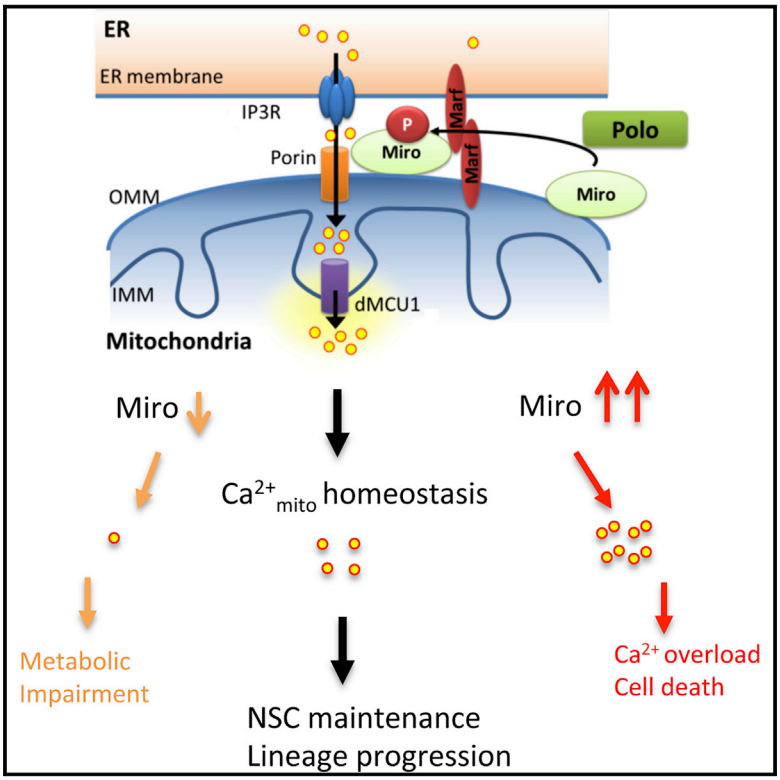

Highlights

- Mitochondrial Rho GTPase Miro regulates NSC maintenance and lineage maturation
- Miro controls mitochondrial Ca^{2+} homeostasis independent of its role in transport
- Miro interacts with Ca^{2+} transporters at the ER-mitochondria contact site
- Miro activity is positively regulated by Polo kinase through phosphorylation

Authors

Seongsoo Lee, Kyu-Sun Lee, Sungun Huh, ..., Seung Hyun Hong, Kweon Yu, Bingwei Lu

Correspondence

bingwei@stanford.edu

In Brief

Lee et al. reveal that mitochondrial Rho GTPase (Miro) is required for maintaining mitochondrial Ca^{2+} homeostasis in *Drosophila* neural stem cell lineages, independent of its role in mitochondrial trafficking. Miro interacts with Ca^{2+} transporters and regulates ER-mitochondria contact site integrity. Its activity is modulated by Polo kinase through direct phosphorylation.

Lee et al., 2016, Developmental Cell *37*, 174–189
April 18, 2016
http://dx.doi.org/10.1016/j.devcel.2016.03.023

CellPress

Developmental Cell
Article

Polo Kinase Phosphorylates Miro to Control ER-Mitochondria Contact Sites and Mitochondrial Ca^{2+} Homeostasis in Neural Stem Cell Development

Seongsoo Lee,[1,2,3,4] Kyu-Sun Lee,[1,2,3] Sungun Huh,[1,3] Song Liu,[1] Do-Yeon Lee,[1] Seung Hyun Hong,[2] Kweon Yu,[2] and Bingwei Lu[1,*]

[1]Department of Pathology, Stanford University School of Medicine, Stanford, CA 94305, USA
[2]BioNanotechnology Research Center, Korea Research Institute of Biotechnology and Bioscience, Daejeon 34141, Korea
[3]Co-first author
[4]Present address: Gwangju Center, Korea Basic Science Institute, Gwangju 61186, Korea
*Correspondence: bingwei@stanford.edu
http://dx.doi.org/10.1016/j.devcel.2016.03.023

SUMMARY

Mitochondria play central roles in buffering intracellular Ca^{2+} transients. While basal mitochondrial Ca^{2+} (Ca^{2+}_{mito}) is needed to maintain organellar physiology, Ca^{2+}_{mito} overload can lead to cell death. How Ca^{2+}_{mito} homeostasis is regulated is not well understood. Here we show that Miro, a known component of the mitochondrial transport machinery, regulates *Drosophila* neural stem cell (NSC) development through Ca^{2+}_{mito} homeostasis control, independent of its role in mitochondrial transport. Miro interacts with Ca^{2+} transporters at the ER-mitochondria contact site (ERMCS). Its inactivation causes Ca^{2+}_{mito} depletion and metabolic impairment, whereas its overexpression results in Ca^{2+}_{mito} overload, mitochondrial morphology change, and apoptotic response. Both conditions impaired NSC lineage progression. Ca^{2+}_{mito} homeostasis is influenced by Polo-mediated phosphorylation of a conserved residue in Miro, which positively regulates Miro localization to, and the integrity of, ERMCS. Our results elucidate a regulatory mechanism underlying Ca^{2+}_{mito} homeostasis and how its dysregulation may affect NSC metabolism/development and contribute to disease.

INTRODUCTION

Mitochondria are important for many aspects of cellular function, from ATP production and intermediary metabolism to apoptosis. Mitochondrial dysfunction has been broadly linked to the pathogenesis of a multitude of neurological disorders (Chan, 2006; Schon and Przedborski, 2011; Tait and Green, 2012; Wallace, 2005), emphasizing the particular importance of this organelle to neuronal function and maintenance. Mitochondrial function and Ca^{2+} signaling have been intimately linked. On one hand, Ca^{2+}_{mito} uptake helps buffer cytosolic Ca^{2+} signals and oscillations such as those generated by neuronal activation, thus amplifying and sustaining signals arising from neuronal activity while protecting neurons from the potentially damaging Ca^{2+} spikes (MacAskill et al., 2010; Sheng and Cai, 2012; Vos et al., 2010). On the other hand, Ca^{2+}_{mito} can positively regulate the activities of tricarboxylic acid (TCA)-cycle enzymes and electron transport chain components, stimulating ATP production (Cardenas et al., 2010; Jouaville et al., 1999; McCormack et al., 1990). Ca^{2+}_{mito} uptake primarily occurs at ERMCS where local Ca^{2+} can reach high levels (Rizzuto et al., 1993, 1998). Proteins localized to ERMCS include those that mediate Ca^{2+} transfer, such as inositol 1,4,5-trisphosphate receptor (IP3R) at the ER, voltage-dependent anion-selective channel (VDAC) at the mitochondria outer membrane (MOM), and mitochondrial Ca^{2+} uniporter (MCU) at the mitochondrial inner membrane (MIM) (Giorgi et al., 2015; Hajnoczky et al., 2002; Rowland and Voeltz, 2012), and mitofusin-2 (de Brito and Scorrano, 2008). In addition to transferring Ca^{2+}, ERMCS also transfers lipids (Hayashi et al., 2009). Despite the importance of ERMCS to fundamental cellular functions and its potential link to disease conditions (Schon and Area-Gomez, 2013; Rizzuto et al., 2012), its roles during normal development remain mostly unexplored, and the signaling mechanisms regulating its integrity and function are largely unknown.

Mitochondrial rho GTPase (Miro) is a MOM protein containing two guanosine triphosphatase (GTPase) domains and two Ca^{2+}-sensing EF-hand domains (Fransson et al., 2003). Genetic studies in *Drosophila* (Guo et al., 2005) and mouse (Nguyen et al., 2014) revealed a key function of Miro in regulating the axonal transport of mitochondria, during which Miro forms a multi-protein complex with Milton and Kinesin heavy chain (KHC) to link mitochondria with motor molecules and the microtubule cytoskeleton (Glater et al., 2006). Through binding to the EF hands of Miro and altering protein-protein interactions within the transport machinery, cytosolic Ca^{2+} dynamically regulates the motility of mitochondria, offering one mechanism to match mitochondrial distribution with neuronal activity (Macaskill et al., 2009; Saotome et al., 2008; Wang and Schwarz, 2009). The PINK1/Parkin pathway, which is critically involved in maintaining mitochondrial function and mutations which are associated with Parkinson's disease, can regulate Miro stability and thus mitochondrial transport (Liu et al., 2012; Wang et al., 2011). Interestingly, despite the importance of the Miro/Milton/Khc complex in regulating mitochondrial transport in metazoans,

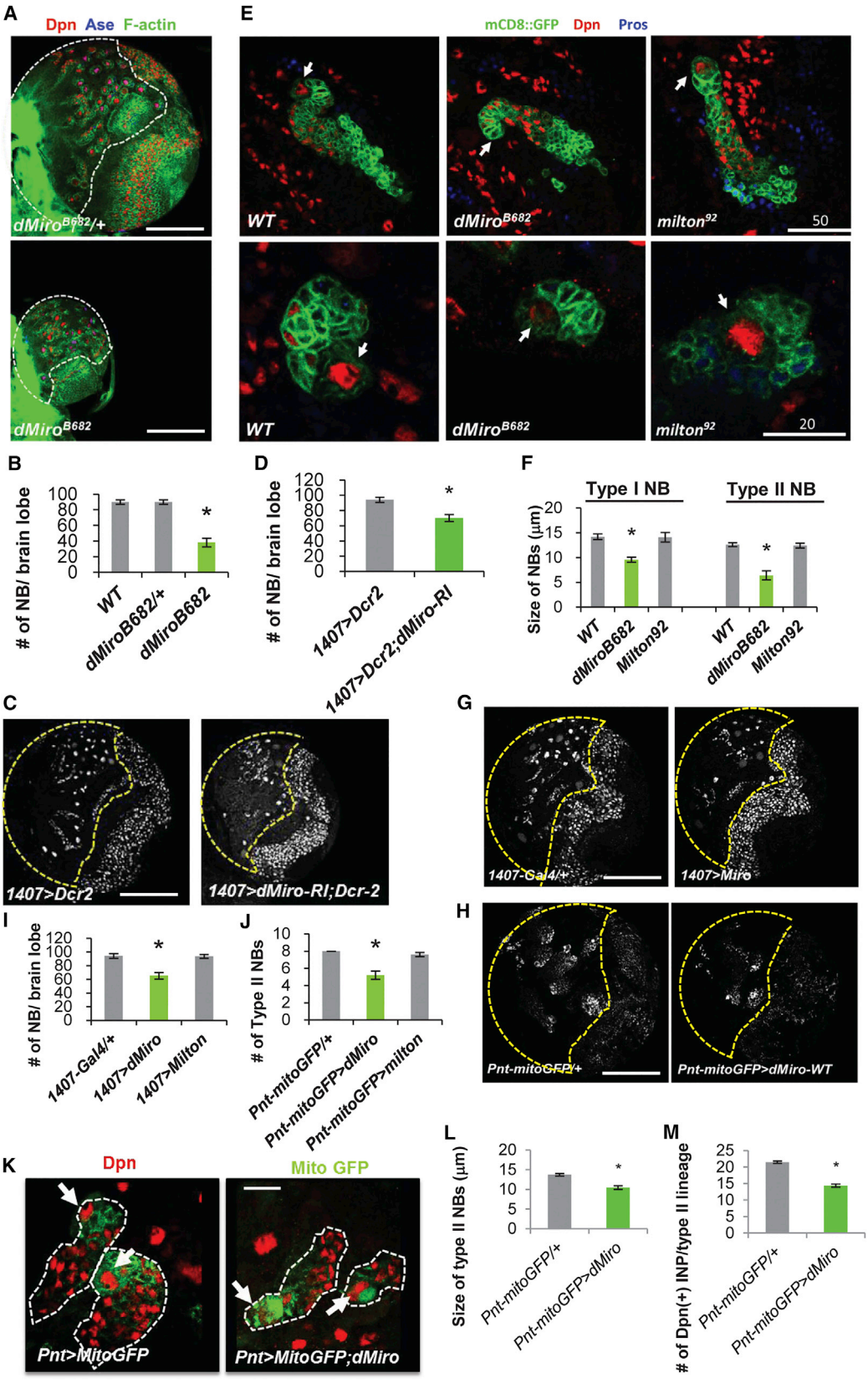

(legend on next page)

Miro is the only component conserved in all eukaryotes, suggesting that it may perform some ancestral function that is independent of the transport complex. Indeed, functions of Miro not directly related to transport are emerging in yeast (Lee and Lu, 2014), where yeast Miro (Gem1) is localized to ERMCS (Kornmann et al., 2011) and regulates ER-associated mitochondrial division (Murley et al., 2013). The prominent roles of Miro in mitochondrial regulation and the importance of mitochondria to neuronal function and survival in humans promoted us to examine the physiological role of Miro in the nervous system of a multicellular organism.

RESULTS

Miro Regulates *Drosophila* NSC Maintenance in a Manner Independent of Mitochondrial Transport

To investigate the physiological function of Miro in a developmental setting, we used *Drosophila* central brain NSCs called neuroblasts (NBs). We examined the type I and type II NBs in the larval brains of animals carrying the $dMiro^{B682}$ mutant allele, presumably a protein null (Figures S1A and S1B) with disrupted mitochondrial distribution in neuronal and muscle tissues and late-larvae or early-pupae lethality (Guo et al., 2005). The brain size and number of Deadpan (Dpn)-positive NBs were dramatically reduced in $dMiro^{B682}$ homozygous mutants (Figures 1A and 1B). Loss of NB was also observed when dMiro was specifically knocked down in the NB lineages by RNAi (Figures 1C and 1D). To examine the effect of *dMiro* mutation on NB-lineage architecture, we performed clonal analysis with MARCM (Lee and Luo, 2001). Type I and type II NB lineages of control animals each invariably contained one Dpn-positive primary NB, whereas the primary NBs were frequently lost in $dMiro^{B682}$ mutant NB clones (Figure 1E). In cases where the primary NBs remained in the mutant clones, their sizes were noticeably smaller than control NBs (Figures 1E and 1F). These results indicate a critical and cell-autonomous role of Miro in the development and/or maintenance of larval brain NBs.

Type II NBs undergo self-renewing asymmetric divisions to generate immature intermediate progenitors (IPs), which progress into transit-amplifying mature IPs that also undergo self-renewing asymmetric divisions to generate ganglion mother cells and differentiated neuronal or glial progenies (Bello et al., 2006; Boone and Doe, 2008; Bowman et al., 2008). IPs sequentially express the transcription factors Dichaete (D), Grainy head (Grh), and Eyeless (Ey) during their transition from young to old IPs (Bayraktar and Doe, 2013). Thus, early-born (old) IPs express Ey, whereas late-born (young) IPs express D. In $dMiro^{B682}$ mutant clones, young IPs and old IPs were both significantly reduced in number compared with control wild-type (WT) clones (Figures S1C and S1D). Loss of function (LOF) of dMiro thus reduces the number of transit-amplifying IPs, presumably as a result of stem cell loss during lineage progression.

Next, we examined the Miro gain-of-function (GOF) effect using *1407-Gal4*-or *Pnt-Gal4*-directed pan-NB or type II NB-specific Miro overexpression (OE), respectively. Miro OE led to a reduction in the number of total NBs in *1407-Gal4>dMiro-OE* (Figures 1G and 1I) and occasional loss of type II NBs under *Pnt-Gal4>dMiro-OE* conditions (Figures 1H and 1J). A reduction in NB size was also seen in dMiro-OE animals (Figures 1K and 1L). In the *Pnt-Gal4>dMiro-OE* condition, the number of IPs, specifically the D^+ young IPs in type II NB lineages, was reduced (Figure 1M). These results indicate that NB maintenance and lineage progression are sensitive to Miro dosage.

Miro is a key component of a conserved protein complex that transports mitochondria along microtubule tracks (Brickley et al., 2005; Fransson et al., 2006; Guo et al., 2005; Hirokawa, 1998; Pilling et al., 2006; Stowers et al., 2002). To test whether the function of Miro in mitochondrial trafficking is important for NB maintenance, we examined mitochondrial distribution in *dMiro* mutant clones by staining for ATPsyn5α. Mitochondrial distribution or morphology was not obviously affected by *dMiro* mutation in NB lineages (Figure S1E). To further assess the role of mitochondrial transport in NB development, we analyzed the LOF and GOF of Milton, another key component of the transport complex (Glater et al., 2006). Neither the number nor size of primary NBs was affected by NB-specific knockdown of Milton (Figure S1F), in $milton^{92}$ mutant MARCM clones (Figures 1E and 1F), or when Milton was overexpressed (Figures 1I and 1J). The *Milton RNAi* line used here was known to be effective in altering neuronal mitochondrial transport or function (Liu et al., 2012; Fang et al., 2012; Iijima-Ando et al., 2009). Intriguingly, Miro OE led to mitochondrial distribution defects in NBs, with mitochondria accumulating asymmetrically to one side of the perinuclear area, and this defect was partially rescued by Milton RNAi (Figure S1G). However, the Miro-OE effect on NB-lineage development was not affected by Milton RNAi (data not shown), suggesting that a transport-independent function of Miro is important for NB maintenance and lineage development.

Figure 1. Regulation of NB Behavior by Miro

(A and B) Reduction of NB number and brain size in $dMiro^{B682}$ null mutant. Larval brains of $dMiro^{B682}$ heterozygous and homozygous animals were immunostained for pan-NB marker Dpn, type I NB marker Ase, and F-actin. The central brain area is outlined by the white dashed line.

(C and D) Reduction of NB number by NB-specific knockdown of dMiro. Control (*1407>Dcr2*) and dMiro RNAi (*1407>Dcr2,dMiro-RI*) larval brains were immunostained for Dpn. The central brain area is outlined with the yellow dashed line.

(E) MARCM analysis of NB lineages in the $dMiro^{B682}$ and $milton^{92}$ backgrounds. Brains were stained for Dpn and Pros, a differentiation marker. NB clones are marked with GFP. Upper: type II NBs. Lower: type I NBs. Primary NBs are indicated with arrows. Note that the primary NB in the $dMiro^{B682}$ type II NB clone is losing Dpn expression.

(F) Quantification of the size of NBs from (E).

(G and H) Effects on NB number by pan-NB (*1407-Gal4*) or type II NB-specific (*Pnt-Gal4*) dMiro OE. Brains were stained for Dpn. The central brain area is outlined by a yellow dashed line.

(I and J) Quantification of total NB (I) or type II NB (J) number from (G) and (H), respectively.

(K–M) Effects of dMiro OE on type II NB size (L) and IP number (M). The type II NB lineages are outlined by a white dashed line. Primary NBs are marked with arrows.

WT, wild-type. Error bars denote SEM; *$p < 0.05$ versus control, Student's t test. n = 5. Scale bars, 100 μm (A, C, G, H) and 20 μm (K). See also Figure S1.

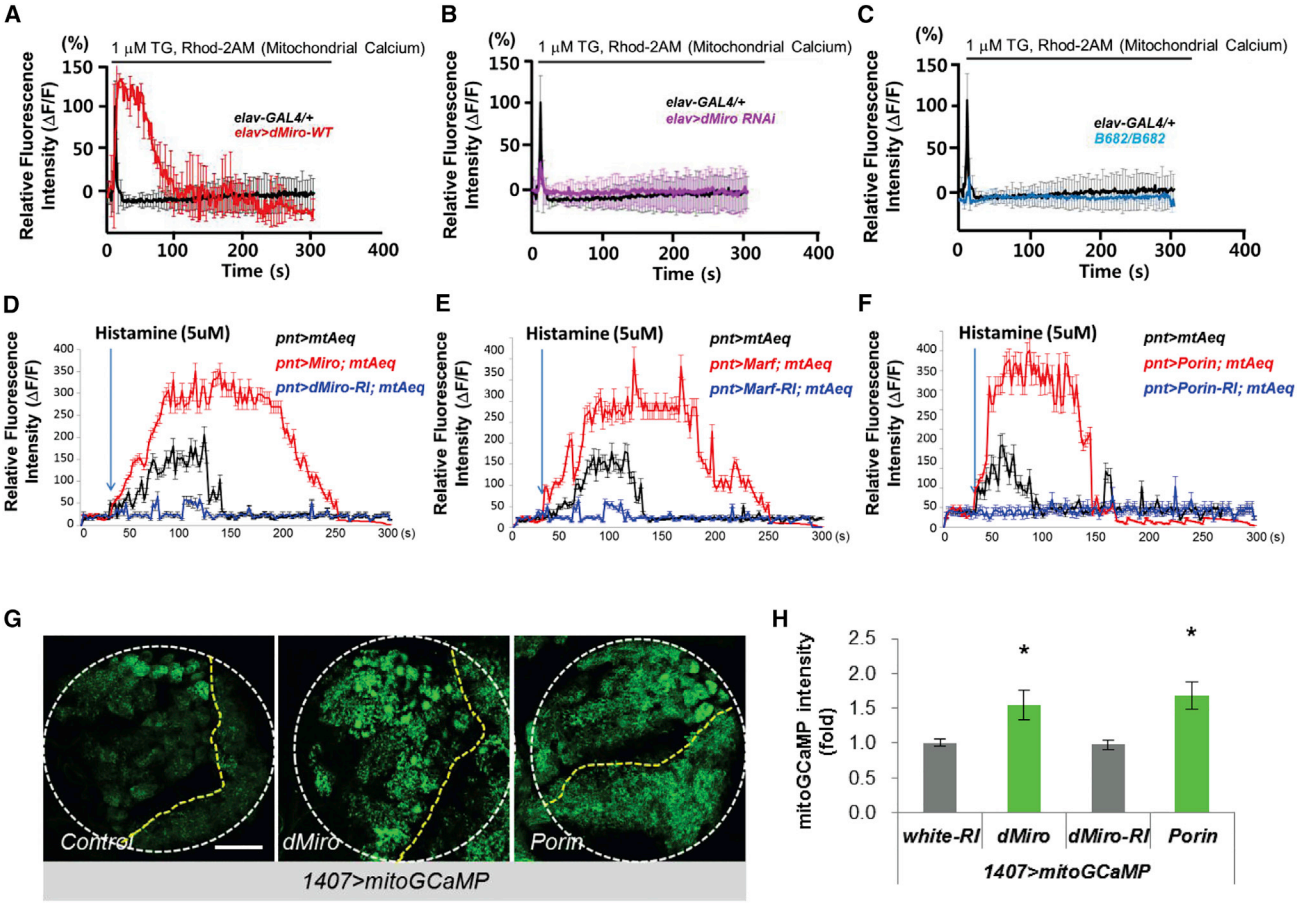

Figure 2. Regulation of Ca^{2+}_{mito} by Miro

(A–C) Effects of pan-neuronal *elav-Gal4* driven dMiro OE (A) or dMiro RNAi (B), or $dMiro^{B682}$ null mutation (C), on TG-stimulated Rhod-2 AM fluorescence in primary cultured fly neurons. The traces show the mean response of cells present in the microscope field and are representative of more than three experiments.

(D–F) Effects of OE or RNAi of Miro (D), Marf (E), or Porin (F) on mitochondrial Ca^{2+} in type II NB lineages as monitored using mtAEQ. The traces show the mean response of ten dissected larval brains present in the microtiter plate and are representative of more than three tests.

(G) Imaging of basal Ca^{2+}_{mito} using mito-GCaMP in larval brains without (control) or with Miro or Porin OE. White circle outlines larval brain, yellow lines separate central brain (left) from the rest of brain. Images are representative of more than five samples. Scale bar, 100 μm.

(H) Quantification of mito-GCaMP intensity in NBs from (G).

Error bars denote SEM. *p < 0.05 versus control, Student's t test. See also Figure S2.

Miro Regulates Ca^{2+}_{mito} Homeostasis

Miro contains GTPase domains and Ca^{2+}-binding EF-hand motifs, and its function in transporting neuronal mitochondria is regulated by activity-induced Ca^{2+} influx (Macaskill et al., 2009; Saotome et al., 2008; Wang and Schwarz, 2009). Yeast Gem1 and mammalian Miro1 (Rhot1) are localized to ERMCS (Kornmann et al., 2011), a structure that directs Ca^{2+} transfer from ER to mitochondria (Hayashi et al., 2009). To test whether Miro regulates Ca^{2+}_{mito} homeostasis in NSC lineage, we first measured Ca^{2+}_{mito} levels under dMiro LOF and GOF, using the Ca^{2+}-sensitive fluorescent dye Rhod-2 AM. Consistent with a previous study (Guo et al., 2005), Rhod-2 AM preferentially monitored Ca^{2+}_{mito} in *Drosophila* neurons (Figure S2A). We loaded primary cultured neurons with Rhod-2 AM. Blocking ER Ca^{2+} uptake with thapsigargin (TG) increased cytosolic Ca^{2+} and induced a spike of Ca^{2+}_{mito} as reported by Perocchi et al. (2010), which quickly dissipated in control cells. Notably, in Miro-OE neurons the TG-induced Rhod-2 AM spike was stronger and persisted longer (Figure 2A), whereas TG induced a much weaker spike in $dMiro^{B682}$ mutant or Miro-RNAi neurons than controls (Figures 2B and 2C). We also measured cytosolic Ca^{2+} response using Fluo-3 AM. OE of WT but not a mutant form of Miro led to a decrease in the magnitude of cytosolic Ca^{2+} spikes induced by TG (Figure S2B).

To detect Ca^{2+}_{mito} levels in vivo in NBs, we expressed genetically encoded, mitochondria-targeted Ca^{2+}_{mito} reporters mito-Apoaequorin (mtAEQ) (Terhzaz et al., 2006) or mito-GCaMP3 (Lutas et al., 2012) in type II NBs. With the mtAEQ reporter, dissected brains from transgenic (Tg) animals were treated with histamine, an IP3-generating agonist, to induce Ca^{2+} release from the ER and increase Ca^{2+}_{mito} uptake (Perocchi et al., 2010), and luminescence signals were immediately measured with an automated luminometer. Under this condition, Ca^{2+}_{mito} was significantly elevated when known components of ERMCS such as Marf and Porin/VDAC were overexpressed, and Ca^{2+}_{mito} was attenuated when they were inhibited (Figures

2E and 2F), validating the utility of the reporters in monitoring the effect of ERMCS on Ca^{2+}_{mito} homeostasis. We found that Ca^{2+}_{mito} was significantly increased by Miro OE but decreased by Miro RNAi (Figure 2D). In contrast, Milton LOF or GOF had no obvious effect on Ca^{2+}_{mito} uptake under similar conditions (Figure S2C). With the mito-GCaMP3 reporter, we observed that basal fluorescence signal was significantly increased by Miro OE or Porin OE (Figures 2G and 2H). The expression level of mito-GCaMP protein was not altered by Miro OE (Figure S2D). These results, and the observations that cytosolic Ca^{2+} level as measured with a cytosolic GCaMP reporter (Figures S2E and S2F), and mitochondrial membrane potential (Figures S2G and S2H), the driving force of Ca^{2+}_{mito} entry, were not altered by Miro OE, support that Miro specifically promotes Ca^{2+}_{mito} uptake. Miro therefore regulates Ca^{2+} transfer from ER to mitochondria, and this occurs in a manner seemingly independent of mitochondrial transport.

Miro-Mediated Ca^{2+}_{mito} Homeostasis Regulates Mitochondrial Activity

Ca^{2+}_{mito} uptake critically regulates many cellular functions, ranging from ATP production to cell death (Rizzuto et al., 2012). Sufficient Ca^{2+} uptake into the mitochondrial matrix is needed for ATP production by enhancing the activities of key metabolic enzymes. For example, the key TCA-cycle enzyme pyruvate dehydrogenase (PDH) is inhibited by phosphorylation by PDH kinase (PDK). Ca^{2+}_{mito} activates PDH phosphatase to remove an inhibitory phosphate from PDHE1 subunit (Cardenas et al., 2010). Thus, Ca^{2+}_{mito} negatively influences p-PDHE1 level. Normalized p-S293-PDHE1 level was markedly increased in *dMiro* mutant but decreased in Miro-OE brain extracts (Figures 3A, 3B, S3A, and S3B). Consistently, the intensity of p-PDHE1 immunosignal was increased in *dMiro* mutant but decreased in Miro-OE NB clones, compared with control NBs located outside of the clones in the same animals (Figure 3C). ATP production in larval brain was decreased in $dMiro^{B682}$ mutant, which was rescued by NB-specific Miro OE (Figure 3G). Measurement of oxygen consumption rate (OCR) confirmed alteration of mitochondrial metabolism under Miro LOF and GOF conditions (Figure 3H). In response to ATP depletion, AMP-activated protein kinase (AMPK) is activated by phosphorylation as a compensatory response to restore energy homeostasis (Hardie, 2007). AMPK was hyperphosphorylated in *dMiro* mutant (Figures 3A and 3B). These results suggest that reduced Ca^{2+}_{mito} uptake impairs mitochondrial metabolism and ATP production under Miro LOF conditions.

While mitochondrial metabolism requires sufficient levels of Ca^{2+}_{mito}, prolonged Ca^{2+}_{mito} uptake can lead to opening of the permeability transition pore and release of pro-apoptotic components such as cytochrome *c*, a critical event in mitochondria-mediated cell death (Rizzuto et al., 2012). To test whether the detrimental effect of Miro OE on NB maintenance is related to Ca^{2+}_{mito} overload-induced cytotoxicity, we analyzed mitochondrial redox status using MitoSOX Red, a mitochondrial superoxide indicator. MitoSOX signal was higher in Miro-OE than control clones. No obvious change in MitoSOX signal was observed in *dMiro* mutant clones (Figures 3D and 3E). Miro-OE but not *dMiro* mutant clones also showed increased staining of activated caspase-3 (Figure 3F), and release of cytochrome *c* into the cytosol (Figures S3C and S3D), which are markers of apoptotic processes.

Under normal physiological conditions, the bulk of cellular Ca^{2+} resides within the ER lumen. ER Ca^{2+} depletion can cause ER stress and activate an unfolded protein response (Malhotra and Kaufman, 2011). We tested whether, by enhancing Ca^{2+}_{mito} uptake, Miro OE might lower ER luminal Ca^{2+} level and cause ER stress. The ER stress marker p-eIF2α was significantly elevated in Miro-OE but not *dMiro* mutant NB clones (Figure S3E), suggesting that elevated Ca^{2+}_{mito} uptake may cause Ca^{2+}_{mito} overload, Ca^{2+} depletion from the ER, and ER stress, all of which may contribute to apoptotic responses in under Miro-OE conditions. To test this hypothesis, we first examined the effect of ER stress inducers on NB development. Acute treatment of third-instar larvae with 5 mM DTT + 1 μM TG resulted in loss of IPs (Figure S3G), indicating that ER stress can recapitulate the Miro-OE effect in NB development. Importantly, two independent RNAi lines against the ER stress kinase PERK both effectively rescued dMiro-OE-induced NB-lineage defects (Figure S3F). Next, we estimated ER Ca^{2+} content by measuring ionomycin-releasable Ca^{2+} levels (Tu et al., 2006). Ionomycin is an ionophore that causes more complete emptying of ER Ca^{2+} stores than TG. In the absence of extracellular Ca^{2+}, ionomycin elevates intracellular (cytosolic) Ca^{2+} by emptying intracellular stores, and the resulting transient Ca^{2+} peak gives a reasonable approximation of steady-state ER Ca^{2+} content. With this method, we found that HeLa cells transfected with hMiro1 have less ER Ca^{2+} content than control cell transfected with empty vector (Figures S3H and S3I). Together, these results indicate that Miro-regulated Ca^{2+} homeostasis within the ER and mitochondria are both important for NB-lineage development.

Miro Interacts with Ca^{2+} Transporters at the ERMCS to Regulate Ca^{2+}_{mito} Homeostasis and NB Maintenance

Transfer of Ca^{2+} from the ER to mitochondria is a major function of the ERMCS carried out by the Ca^{2+} transporters IP3R, VDAC, and MCU localized at the ER, MOM, and MIM, respectively. We found that similarly to the Miro case, knocking down fly IP3R (Venkatesh and Hasan, 1997), Porin (VDAC) (Messina et al., 1996), or MCU resulted in reduced NB number (Figures S4A–S4D), supporting the importance of ER-mitochondria Ca^{2+} transfer to NB maintenance. In addition, overexpressing these Ca^{2+} transporters also modestly reduced NB number (Figures S4E and S4F). We further tested the genetic interaction between Miro and the Ca^{2+} transporters. Although the heterozygous conditions for *dMiro* or each of the Ca^{2+} transporter genes alone had no obvious effect on NB development, double heterozygous combinations between *dMiro* and the Ca^{2+} transporters resulted in reduced NB number (Figures 4A and 4B), supporting that Miro functionally interacts with Ca^{2+} transporters at the ERMCS to control Ca^{2+}_{mito} homeostasis, mitochondrial function, and NB maintenance. Consistently, partial LOF of IP3R or Porin reduced Ca^{2+}_{mito} to basal levels under Miro-OE conditions and blocked the Miro-OE effect on NB maintenance (Figures S4G and S4H).

We next took a pharmacological approach to test the role of Ca^{2+}_{mito} homeostasis in mediating Miro function in NSCs. Previous studies showed that feeding flies with $CaCl_2$ could increase intracellular Ca^{2+} levels, especially at the larval stage (Dube et al., 2000), and that exogenous Ca^{2+} could overcome genetic deficits

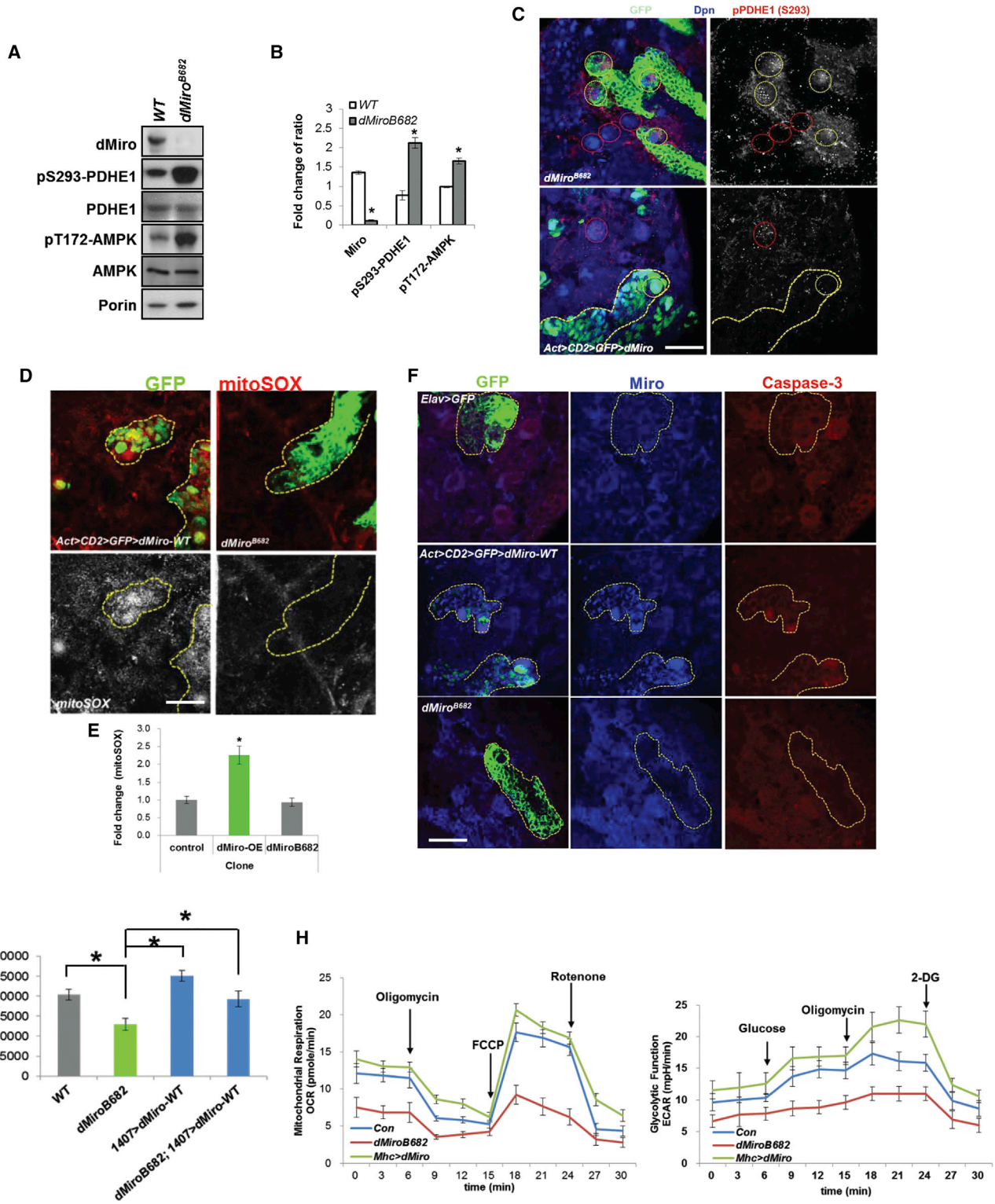

Figure 3. Miro-Mediated Ca^{2+}_{mito} Homeostasis Regulates Mitochondrial Activity

(A and B) Western blot (WB) analysis (A) showing increased p-PDHE1 and p-AMPK in *dMiro* mutant. PDHE1, AMPK, Porin, and actin serve as controls. Normalized protein levels (B) are shown as the ratio of dMiro/Porin, pS293-PDHE1/PDHE1, and pT713-AMPK/AMPK from (A).

(C–F) Immunostaining of p-PDHE1 (C), mito-SOX (D and E), or activated caspase 3 (F) in *dMiro* mutant MARCM clones (outlined in yellow in upper panels) or dMiro-OE flip-out clones (outlined in yellow in lower panels). NBs within clones are marked with white circles, and control NBs outside of the clones are marked with red circles in (C).

(legend continued on next page)

in intracellular Ca^{2+} signaling (Howard, 1984). We found that Ca^{2+}_{mito} was increased upon $CaCl_2$ feeding (Figures S4I and S4J), and that feeding *dMiro*^{B682} mutant larvae with $CaCl_2$ partially restored ATP production (Figure 4C) and rescued the brain size reduction and NB loss (Figure 4D). Conversely, Ca^{2+}_{mito} overload caused by Miro OE was attenuated (Figures S4I and S4J), and the reduction of NB size and loss of IPs in the *Pnt>Miro-OE* condition was rescued by reducing the Ca^{2+}_{mito} level via Ca^{2+}chelation with bis(2-aminophenoxy)ethane tetra-acetic acid (BAPTA), or IP3R inhibition with 2-aminoethoxydiphenyl borate (2-APB) (Figures 4E and 4F).

We also tested the interaction between Miro and the ER-mitochondria Ca^{2+} transporters using available GOF alleles. NB-specific OE of Porin or dMCU significantly rescued the NB-loss phenotype seen in *dMiro*^{B682} mutant (Figures 4G and 4H). Consistent with mitochondrial metabolic impairment due to reduced Ca^{2+}_{mito} uptake being responsible for the NB phenotype in *dMiro*^{B682} mutant, OE of yeast NDI1 (yNDI1), which encodes a single-peptide alternative complex I and is functional in boosting fly mitochondrial complex I activity (Bahadorani et al., 2010; Sanz et al., 2010), partially restored NB number in *dMiro*^{B682} mutant. Enhancing PDH activity by PDK RNAi had a similar effect (Figures 4G and 4H). This contrasts with the lack of effect of overexpressing the apoptosis inhibitor p35 (data not shown), or the compound removal of three cell-death executors in flies (Reaper, Grim, and Hid) using the *H99* deficiency (Foley and Cooley, 1998) (Figures 4G and 4H). These results support the notion that the Miro LOF effect on NB maintenance is due to Ca^{2+}_{mito} depletion and metabolic impairment as opposed to Ca^{2+}_{mito} overload and apoptotic activation under Miro GOF conditions.

Regulation of Miro Function by Polo-Mediated Phosphorylation at Serine 66

Despite the importance of ER-mitochondria Ca^{2+} signaling to cellular physiology, little is known how this process is regulated. Implication of Miro as a key player in this process offers the opportunity to investigate the regulatory mechanisms. By aligning the sequence of Miro homologs from fly to humans, we identified a conserved, putative phosphorylation site for Polo-like kinases (PLKs) in the N-terminal GTPase domain of Miro (Figures 5A and S5A). Of the two GTPase domains of Miro, the N-terminal one is particularly important for ERMCS localization (Kornmann et al., 2011), mitochondrial morphology and transport, and cell survival (Babic et al., 2015). Polo is also of particular interest, as previous studies identified it as a regulator of NB self-renewal in *Drosophila* (Wang et al., 2007). Our immunohistochemical and biochemical analyses indicated that a fraction of Polo protein is localized to mitochondria (Figures S5B–S5E). To test for a molecular link between Miro and Polo in NB maintenance, we first asked whether Miro and Polo physically interact in vivo. In coIP experiments using *elav>Polo-GFP* fly head extracts, we detected Polo-GFP in complex with endogenous dMiro (Figure 5B). Co-expression with Polo resulted in increased dMiro phosphorylation at Ser but not Thr residue(s) (Figures 5C and 5D). To test whether Polo directly phosphorylates Miro, we performed in vitro kinase assays using PLK1 as kinase and GST-dMiro fusion proteins as substrates. PLK1 strongly phosphorylated Miro-FL (amino acids [aa] 1–634) and Miro-N (aa 1–213), but not Miro-M (aa 210–393) or Miro-C (aa 390–634) (Figure 5E). None of the GST-Miro fusion proteins was phosphorylated by a control kinase, protein kinase C ζ (PKCζ) (Figures S5F and S5G). We next searched for the target site of Polo in Miro-N by focusing on conserved Ser residues, including Ser66 that matches the consensus site for PLKs (Figures 5A and S5A). We note that the corresponding sites in mammalian Miro1 and Miro2 may be better targets for PLK2 or 3, which prefers an acidic residue at the +1 position (Rozeboom and Pak, 2012). An S66A mutation led to a dramatic reduction of Miro-N phosphorylation by PLK1 compared with mutating other conserved Ser residues (Figure 5F). S66 in dMiro-N-terminal GTPase domain thus represents a major phosphorylation site for PLK1 in vitro.

To study the physiological effects of Polo-mediated phosphorylation of Miro in vivo, we generated Tgs expressing WT dMiro (dMiro-WT) or dMiro-S66A. To circumvent OE artifacts, we chose for further analyses Tgs that express dMiro-WT and dMiro-S66A at comparable, but less than endogenous dMiro expression levels (Figures 6F and S3A). The NB-loss phenotype seen in *dMiro* mutant was significantly rescued by *1407-Gal4*-driven expression of dMiro-WT but not dMiro-S66A (Figures 5G and 5H). This effect is likely related to the function of Miro in modulating Ca^{2+}_{mito} homeostasis, as dMiro-S66A exhibited compromised ability to induce Ca^{2+}_{mito} uptake compared with dMiro-WT (Figures S5H and S2B). Similarly, reduced ATP production in *dMiro* mutant larval brain was rescued by *1407-Gal4*-driven dMiro-WT, but not -S66A (Figure 5I). Unlike in dMiro-WT case, NB clones overexpressing dMiro-S66A did not show increased mitochondrial reactive oxygen species (Figure S5J). Phosphorylation of S66 in dMiro thus positively influences its function in regulating mitochondrial function and NB maintenance under basal conditions.

Consistent with Polo playing a role in regulating Ca^{2+}_{mito} homeostasis, Ca^{2+}_{mito} level was increased by Polo OE but moderately decreased by Polo RNAi (Figure S5I). Moreover, constitutively active Polo (Polo-CA) caused significant loss of type II NBs and IPs, which was rescued by dMiro RNAi or dMiro-S66A co-expression (Figures 5J–5L), or by RNAi of genes mediating ER-mitochondria Ca^{2+} transfer (Figures 5M and 5N). Importantly, the NB and IP loss caused by Polo OE was also partially rescued by pharmacological interventions that reduce Ca^{2+}_{mito} (Figures S5K and S5L). This effect was specific, as NB and IP losses caused by Numb OE (Ouyang et al., 2011) was not rescued by similar treatments (Figure S5M). The Polo-Miro axis thus plays a physiological role in regulating NB maintenance via Ca^{2+}_{mito} homeostasis.

Phosphorylation of Miro by Polo Regulates the Integrity of ERMCS

We next sought to understand the mechanism by which Polo phosphorylation of Miro affects Ca^{2+}_{mito} homeostasis. We first

(G) Effect of dMiro-WT OE on ATP level in *dMiro* mutant larval brain.

(H) Real-time changes in OCR and glycolytic rate (ECAR) were measured in control, dMiro-WT-OE (*Mhc>dMiro-WT*), and *dMiro* mutant animals using the Seahorse Bioscience XF Analyzer.

Error bars denote SEM. *p < 0.05 versus control, Student's t test. Scale bars, 50 μm (C) and 20 μm (D and F). See also Figure S3.

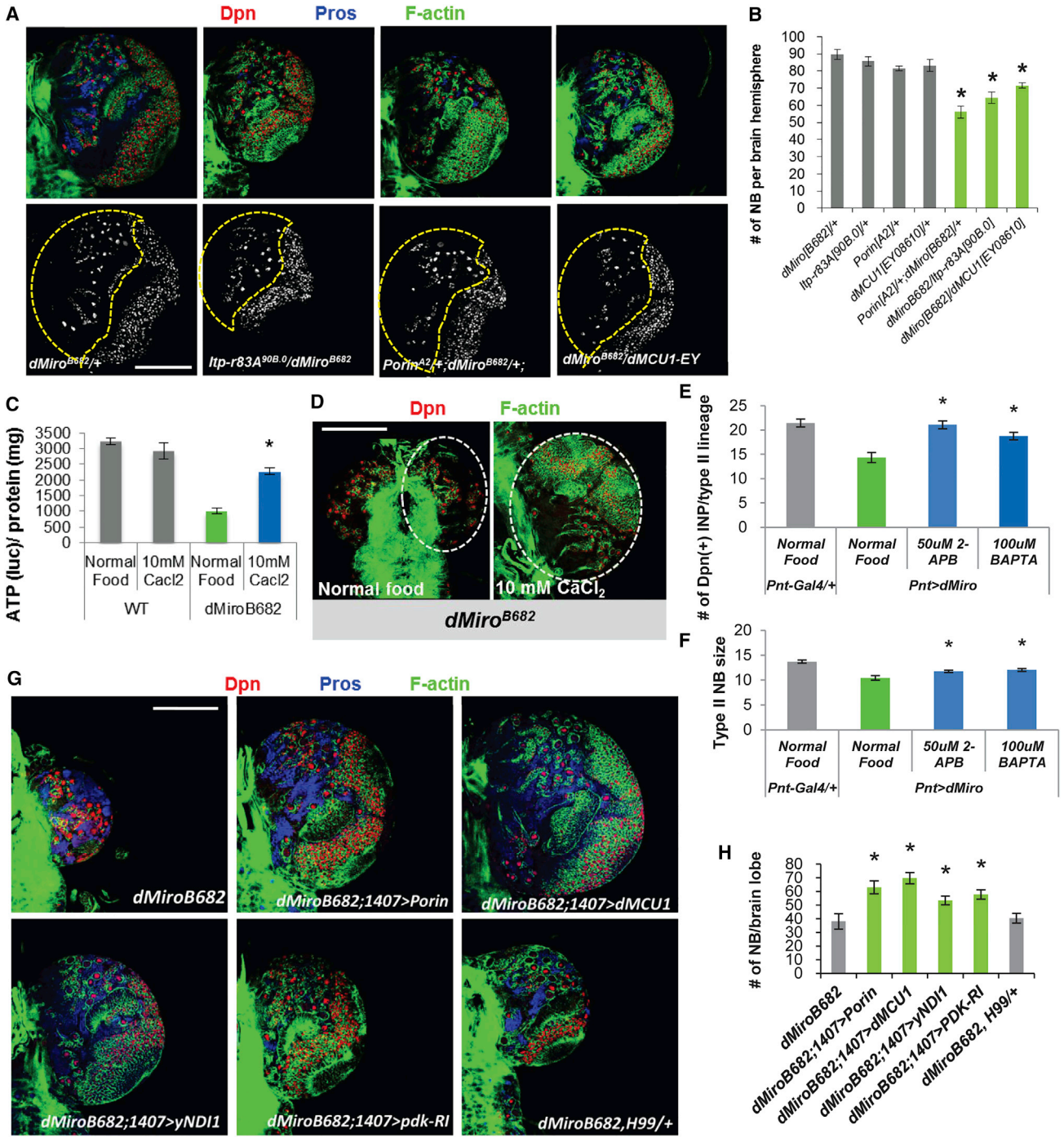

Figure 4. Functional Interaction between Miro and Ca^{2+} Transporter at the ERMCS

(A and B) Transheterozygotes between *dMiro* and *IP3R* (*Itp-r83A*), *Porin*, or *dMCU* mutants resulted in reduction of NB number. Larval brains were immunostained for Dpn, Pros, and F-actin (cell cortex). Central brain area is outlined with dashed line.

(C and D) Effects of $CaCl_2$ feeding in rescuing brain ATP level (C) and brain size (D) of *dMiro* mutant. Larval brains were immunostained for Dpn and F-actin. Brain lobes are outlined.

(E and F) Quantification of the effects of 2-APB and BAPTA feeding in rescuing the reduced IP number (E) and NB size (F) caused by dMiro OE.

(G) Genetic interactions showing rescue of NB number in *dMiro* mutant by the OE of Porin, dMCU, yNDI1, or PDK RNAi, but not the *H99* heterozygous background. Larval brains were immunostained for Dpn, Pros, and F-actin.

(H) Quantification of number of NBs shown in (G).

Error bars denote SEM. *p < 0.05, Student's t test. Scale bars, 100 μm. See also Figure S4.

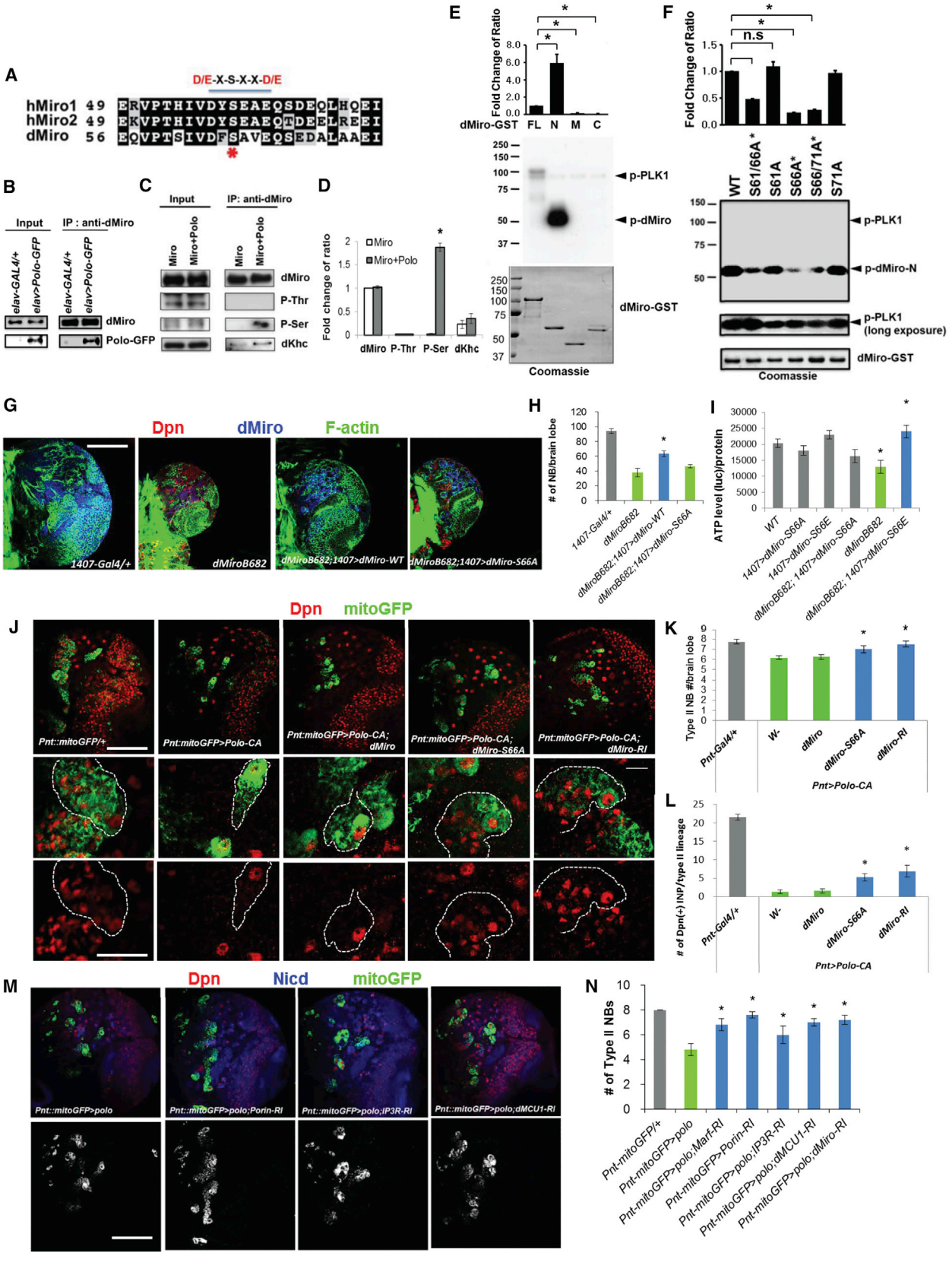

(legend on next page)

tested whether phosphorylation affects the localization of Miro. For this purpose, we generated an antibody against dMiro phosphorylated at S66 (p-S66-Miro), the specificity of which was demonstrated by the absence of signal in *dMiro* mutant (Figures S6A–S6C), its sensitivity to phosphatase treatment (Figure S6D), and its response to altered Polo activity (see later). To specifically examine the localization of Miro or p-S66-Miro with respect to mitochondria and ER, we used RFP tagged with the ER-retention sequence KDEL, or ER resident protein PDI tagged with GFP as ER markers, and ATPsyn5α as mitochondrial marker. Compared with the rather uniform mitochondrial localization of Miro protein in general, p-S66-Miro exhibited a granular localization pattern that co-localized with ATPsyn5α and overlapped extensively with ER markers in the perinuclear area (Figures 6A, 6B, and 6D). The abundance of p-S66-Miro in the perinuclear area was reduced by Polo RNAi but increased by Polo-WT or Polo-CA OE (Figures 6C and 6E). Phosphorylation of Miro by Polo at S66 thus promotes its localization to the ERMCS.

To test whether Miro interacts with proteins localized to ERMCS and whether this interaction is affected by its phosphorylation status, we performed coIP assays using fly brain tissues expressing dMiro-WT, dMiro-S66A, or phosphomimetic dMiro-S66E, which functioned similarly to dMiro-WT in NBs when overexpressed (Figures 6F and 5I). Tg expression was driven by the pan-neuronal *elav-Gal4* driver. Miro-WT exhibited physical association with VDAC/Porin and Mitofusin/Marf, two key components of the ERMCS (de Brito and Scorrano, 2008; Rowland and Voeltz, 2012). Importantly, the Miro-Porin and Miro-Marf interactions were significantly enhanced by S66E, whereas the Miro-Marf interaction was attenuated by S66A mutation (Figures 6F and 6H), suggesting that S66 phosphorylation positively influences the interaction of Miro with proteins at the ERMCS.

We next examined the effect of Miro phosphorylation on ERMCS integrity. To this end, we analyzed the IP3R-VDAC interaction in brain tissues of *dMiro* mutant or Tg flies expressing Miro variants. Although the expression level of IP3R or VDAC was unaltered in all genotypes tested, their physical association was reduced in *dMiro* mutant or Miro-S66A Tg tissues, but increased in Miro-WT or Miro-S66E Tg tissues (Figures 6G and 6I). Since S66 is located within the first GTPase domain of Miro, we examined the effect of S66 phosphorylation status on GTPase activity. In vitro GTPase assays showed time-dependent GTP hydrolysis by the N-terminal GTPase domain of Miro-WT and Miro-S66D or Miro-S66E, with phosphomimetic Miro exhibiting greater GTPase activity than Miro-WT (Figure S6E). Moreover, prior phosphorylation by Polo significantly enhanced the GTPase activity of Miro-WT but not Miro-S66A (Figure S6F). We conclude that Polo-mediated phosphorylation positively regulates the GTPase activity of Miro and the recruitment of Miro to ERMCS, where p-S66-Miro enhances the integrity of this ER-mitochondria tethering complex.

Miro Plays Conserved Roles in Regulating Ca^{2+}_{mito} Homeostasis in Mammalian Cells

To test the conservation of the mechanisms of Miro function and regulation, we turned to the human cervical cancer cell line (HeLa) and mouse NSCs. Addition of IP3R agonist histamine to HeLa cells enhanced the recruitment of hMiro1 to the perinuclear ER area, and this effect was ameliorated by co-treatment with BI2536, a specific chemical inhibitor of PLK1 (Figures 7A, 7B, and S7B). Monitoring Ca^{2+}_{mito} with Rhod-2 AM showed that Ca^{2+}_{mito} was significantly increased in cells transfected with dMiro-WT or -S66E, but less so with dMiro-S66A (Figures 7C and 7D). Previous studies showed that hMiro1 (Fransson et al., 2003) or dMiro (Liu et al., 2012) caused aberrant mitochondrial morphology when overexpressed. We found that hMiro1-induced mitochondrial aggregation in HeLa cells was attenuated by treatment with 2-APB or Ru360, cell-permeant pharmacological inhibitor of IP3R or MCU, respectively (Tang et al., 2005; Garcia-Rivas Gde et al., 2006), or by chelating Ca^{2+} with BAPTA-AM (Figure 7E), suggesting that Miro-regulated Ca^{2+}_{mito} homeostasis underlies its effect on mitochondrial morphology. Moreover, Myc-tagged dMiro-WT, -S66E, or -S66D exhibited more pronounced perinuclear and aggregated localization than Miro-S66A (Figure S7C). These results suggest that as in fly tissues, phosphorylation of Miro at S66 site promotes Miro localization to ERMCS in HeLa cells. We also examined the effect of Polo-Miro signaling on the integrity of the ER-mitochondria tethering complexes. The interaction between VDAC and IP3R was weakened by treatment with BI2536 (Figures 7F and 7G). Immunostaining with ER and mitochondrial markers reveal that ER-mitochondria interaction was increased in cells transfected with hMiro1-WT but not with hMiro1-SA (Figures S7E and S7F), supporting a critical role of PLK signaling in ER-mitochondria interaction and Ca^{2+}_{mito} uptake. Finally, we examined the effect of

Figure 5. Regulation of Miro Function by Polo-Mediated Phosphorylation at Serine 66

(A) Comparison of candidate Polo/PLK phosphorylation motifs at the N terminus of Miro. The consensus D/E-X-S-X-X-D/E motif is underlined and S66 is indicated by an asterisk.

(B) Polo-GFP is present in dMiro IP prepared from fly brain extracts.

(C and D) Increased dMiro phosphorylation at Ser but not Thr residue(s) after Polo co-expression in fly brain. (D) Quantification of normalized phospho-Ser intensity from (C).

(E and F) In vitro kinase assays showing phosphorylation of dMiro-N by PLK1 (E), and the strong effect of S66A mutation in blocking PLK1 effect (F). Bar graph shows quantification of normalized phospho-dMiro signal (top). GST-dMiro proteins were visualized by autoradiography (middle) or Coomassie blue staining (bottom).

(G and H) Rescue of brain size (G) and NB number (H) in *dMiro* mutant by dMiro-WT but not -S66A. Larval brains were immunostained for Dpn, dMiro, and F-actin.

(I) Rescue of reduced brain ATP level in *dMiro* mutant by dMiro-S66E but not -S66A.

(J–L) Rescue of type II NB number (J and K) or IP number (J and L) in Polo-CA OE animals by dMiro-S66A or dMiro RNAi. Larval brains were immunostained for Dpn and GFP. Dashed lines mark type II NB lineages.

(M) Rescue of type II NB number in Polo OE animals by RNAi of ERMCS components. Larval brains were immunostained for Dpn, GFP and NICD (cell membrane).

(N) Quantification of number of NBs in (M).

Error bars denote SEM. *$p < 0.05$, Student's t test. Scale bars, 100 μm (G, upper panel of J, M), 20 μm (lower panel of J). See also Figure S5.

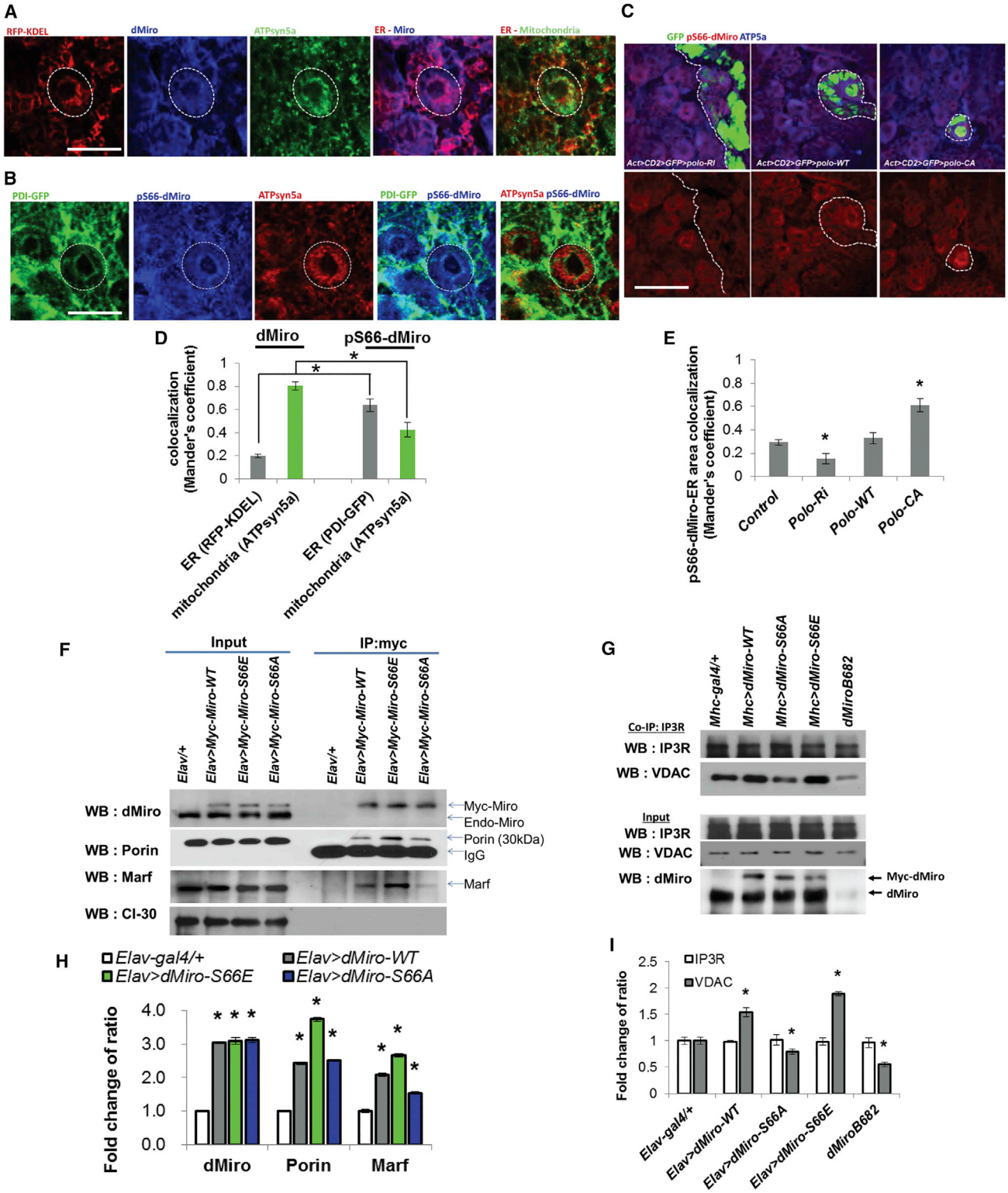

Figure 6. Phosphorylation of Miro Regulates the Integrity of ERMCS

(A and B) Immunostaining showing localization of p-S66-Miro to ERMCS of larval brain NBs. Circles mark the NBs of interest. Larval brains were stained for the indicated antibodies.

(C) Effects of Polo on p-S66-Miro immunosignal in flip-out NB clones with Polo overexpressed or knocked down by RNAi. Clones are marked with GFP and outlined with white dashed lines.

(legend continued on next page)

Miro on the proliferation of mouse NSCs. Transfection of NSCs with hMiro1-WT attenuated NSC proliferation, whereas hMiro1-S59A (equivalent of dMiro-S66A) was less effective in this aspect (Figure 7H). Mitochondrial metabolism as monitored by OCR was increased by hMiro1-WT but decreased by hMiro1-SA in mouse NSCs (Figure S7G). Supporting the importance of ER-mitochondria Ca^{2+} transfer in NSC regulation, pharmacological inhibition of Ca^{2+}_{mito} uptake by Ru360, and to a lesser extent by 2-APB, attenuated NSC proliferation (Figure S7D).

DISCUSSION

Mitochondrial and Ca^{2+} signaling pathways are intimately connected in many aspects of cellular physiology, from metabolism and ATP production to cell death. Previous studies have emphasized the key role of Miro in regulating mitochondrial transport by sensing local elevation of cytosolic Ca^{2+} concentration elicited by neuronal activity. This mechanism links mitochondrial distribution to the subcellular need for Ca^{2+} buffering. In this study we demonstrate a conserved role of Miro in regulating Ca^{2+}_{mito} homeostasis in an apparently transport-independent manner. Miro localizes to ERMCS and interacts with its protein components. We further show that this function of Miro is regulated by Polo-mediated phosphorylation at a conserved site in the N-terminal GTPase domain. The identification of new regulators of Ca^{2+}_{mito} homeostasis offers the opportunity to elucidate how Ca^{2+}_{mito} uptake is controlled in different cell types of multicellular organisms, and how defects in this process may affect development and disease.

Our results identify the Polo/Miro signaling axis as an important regulator of Ca^{2+}_{mito} uptake. ER is a major source of Ca^{2+}_{mito}, which is transported to mitochondrial matrix through Ca^{2+} transporters located at the ERMCS. Despite detailed biophysical studies of Ca^{2+}_{mito} uptake, little is known about how this process is regulated to meet the developmental and physiological needs of distinct cell types in a multicellular organism. We show that Miro is localized to ERMCS, where it interacts with components of the ERMCS to modulate the integrity of this quasi-synaptic structure and the inter-organelle Ca^{2+} transfer. Our genetic and biochemical studies further identify Polo kinase as a key regulator of Miro-controlled Ca^{2+}_{mito} homeostasis. Polo-induced phosphorylation of Miro promotes the localization of Miro to ERMCS, enhancing the interaction between Miro and components of the ER-mitochondria tethering complex and the integrity of the tethering complex. Our identification of S66 in the N-terminal GTPase domain as a key regulatory site of Miro is consistent with the known importance of this GTPase domain to Miro function (Kornmann et al., 2011; Babic et al., 2015). Our results also uncover a new mechanism of action for Polo in NSC self-renewal and differentiation. Dysregulation of PLKs has been implicated in cancer (Craig et al., 2014) and neurodegenerative diseases such as Parkinson's disease (Mbefo et al., 2010). Given that Miro-OE-induced cell death involves Ca^{2+}_{mito} overload, mitochondrial dysfunction, oxidative stress, ER stress, and caspase-3 activation, key features broadly implicated in neurodegenerative diseases, it would be interesting to test in various disease conditions whether disease-causing genes or signaling pathways converge on Miro, and whether pharmacological inhibition of PLK-Miro signaling may offer broad therapeutic benefits.

Our analyses of the effect of Miro LOF and GOF in the fly NB lineages reveal a critical role of Ca^{2+}_{mito} homeostasis in cell fate determination. Miro LOF and GOF both impair NB maintenance and lineage development, but through different mechanisms. Miro LOF causes Ca^{2+}_{mito} depletion and reduced ATP production, impairing cell growth, a key requirement of NB maintenance (Song and Lu, 2011), and causing premature differentiation and loss of NB stemness through a non-apoptotic mechanism. In contrast, Miro GOF causes Ca^{2+}_{mito} overload, oxidative stress, and activation of the apoptotic cascade, leading to failed maintenance of NB and IPs. These results reveal hypersensitivity of NSC maintenance and lineage progression to Ca^{2+}_{mito} levels. A role for Ca^{2+} signaling in progenitor maintenance was previously shown in the fly hematopoietic system (Shim et al., 2013). However, distinct from the importance of Ca^{2+}_{mito} to NB maintenance reported here, the maintenance of hematopoietic progenitors involves cytosolic Ca^{2+}, which is mediated by CaMKII signaling and is sensitive to SERCA (sarco-/endoplasmic reticulum Ca^{2+}-ATPase) activity (Shim et al., 2013), whereas NSC maintenance by Miro-mediated Ca^{2+}_{mito} homeostasis is insensitive to SERCA manipulation (data not shown). Together with previous studies implicating mitochondrial regulators or structural proteins in stem cell differentiation (Kasahara et al., 2013; Mitra et al., 2012; Lee et al., 2013; Teixeira et al., 2015), our result broadens the impact of mitochondria on developmental processes. Given the emerging connection between mitochondrial metabolism and epigenetic modifications (Wallace, 2010; Castegna et al., 2015), we speculate that there exists a mechanistic link between Miro-controlled Ca^{2+}_{mito} homeostasis and epigenetic regulation in the nucleus. Future studies will establish, at the molecular level, how developmental pathways dictating stem cell self-renewal versus differentiation decision are connected with signaling pathways regulating mitochondrial function.

EXPERIMENTAL PROCEDURES

Fly Genetics

Fly culture and crosses were performed according to standard procedures and raised at indicated temperatures. For generation of *UAS-dMiro-S66A* and *UAS-dMiro-S66E* Tg flies, WT *dMiro* cDNA was modified using the QuikChange Multi kit (Stratagene) to introduce the S66A and S66E mutations. The insert of *UAS-dMiro-WT-Myc* was replaced with *dMiro-S66A* and *dMiro-S66E* cDNAs to generate *UAS-dMiro-S66A-Myc* and *UAS-dMiro-S66E-Myc*,

(D and E) Quantification of dMiro and p-dMiro co-localization with ER and mitochondria shown in (A) and (B) (D) or p-dMiro co-localization with ER shown in (C) (E), using Manders' coefficient.

(F) CoIP assays showing the effects of S66A and S66E mutations on Miro interaction with Porin and Marf.

(G) CoIP assays showing the effects of *dMiro* mutation or OE of Miro variants on IP3R-VDAC interaction.

(H) Quantification of proteins pulled down by coIP in (F).

(I) Quantification of proteins pulled down by coIP in (G).

Error bars denote SEM. *$p < 0.05$, Student's t test. Scale bars, 20 μm. See also Figure S6.

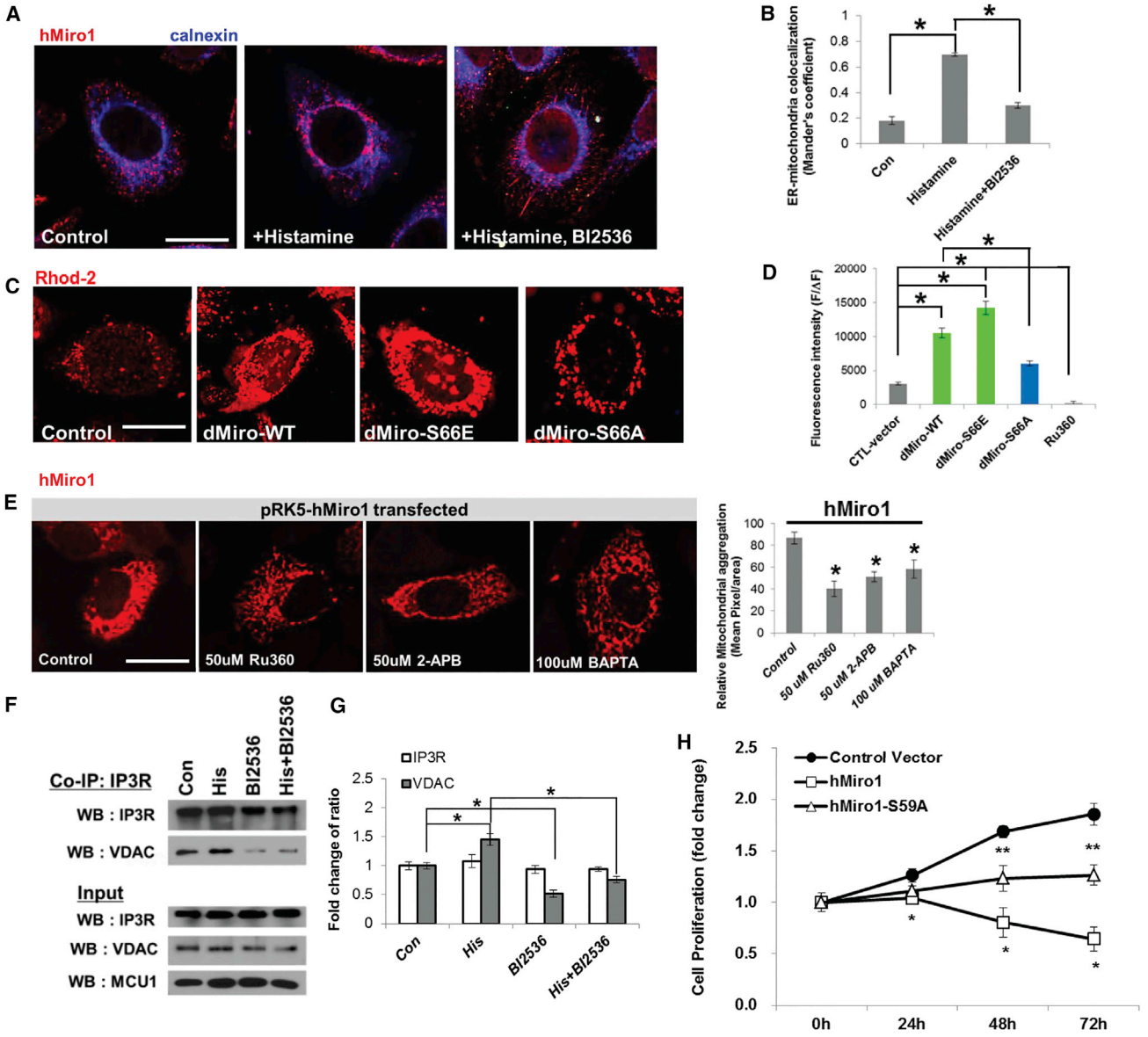

Figure 7. Regulation of Ca^{2+}_{mito} by Miro in Mammalian Cells

(A) Immunostaining showing that the PLK inhibitor BI2536 blocked histamine-induced hMiro1 recruitment to perinuclear ER area in HeLa cells.
(B) Quantification of Miro-Calnexin co-localization using Manders' coefficient.
(C) Effects of dMiro variants on Rhod-2 AM fluorescence in HeLa cells.
(D) Quantification of Rhod-2 signals. RU360 treatment serves as control.
(E) Effects of pharmacological intervention of ER-mitochondrial Ca^{2+} transfer (RU360, 2-APB) or Ca^{2+} availability (BAPTA) on hMiro1-induced mitochondrial morphology change visualized with mitochondria-localized hMiro. Bar graph shows quantification of mitochondrial aggregation.
(F) CoIP assay showing effect of PLK inhibition on IP3R-VDAC interaction in HeLa cells.
(G) Quantification of signal intensity change shown in (F).
(H) Effects of hMiro1-WT and hMiro1-S59A transfection on mammalian NSC (ReNcell CX) proliferation monitored over a 72-hr time course.
Error bars denote SEM. *$p < 0.05$, **$p < 0.01$, Student's t test. Scale bars, 100 μm. See also Figure S7.

respectively. The resulting *pUAST-Miro* constructs were injected into w^- embryos to obtain Tg lines according to established procedures (Bestgene).

MARCM and Flip-Out Clonal Analysis

For generation of NB MARCM clones and OE clones, larvae at 24 hr after larvae hatching (ALH) were heat-shocked at 37°C for 90 min and further aged for 72 hr at 25°C before dissection. MARCM analyses were performed essentially as described by Song and Lu (2011). For the production of OE clones, *w*, *hsFLP*; *Actin 5c>CD2>Gal4*, *UAS-GFP-NLS* was crossed with the indicated *UAS* lines, and 24 hr ALH larvae were heat-shocked at 37°C for 90 min and further aged for 72 hr at 25°C before dissection.

Pharmacological Treatment

2-APB (Sigma), Ru360 (Calbiochem), EDTA/EGTA (Sigma), $CaCl_2$ (Sigma), BAPTA (Life Technologies), histamine (Sigma), thapsigargin (Calbiochem), or BI2536 (Selleckchem) dissolved in 0.5% DMSO was mixed in instant *Drosophila*

medium or cell culture at the indicated final concentrations. 0.5% DMSO alone was used as vehicle control. For treatment of flies, embryos were collected on drug-containing food or control food for 6 hr at 25°C and allowed to develop further to 120 hr ALH before larval brain dissection and immunostaining.

Immunohistochemistry

To generate the p-S66 Miro antibody, we used a synthetic peptide with the sequence SIVDFpSAVEQS to elicit an immune response in rabbits. Purification of the phospho-specific antibody was performed by AbFrontier. Purified p-S66 antibody was diluted at 1:200 for immunostaining. For larval brain immunostaining, larvae were dissected in Schneider's medium (Invitrogen) and fixed with 4% formaldehyde in PEM buffer (100 mM PIPES [pH 6.9], 1 mM EGTA, 1 mM $MgCl_2$) for 23 min at room temperature. For ER-mitochondria interaction analysis, confocal image stacks were automatically thresholded using ImageJ. Co-localization between organelles was quantified using Manders' algorithm (Manders et al., 1993).

Co-immunoprecipitation and Western Blot Analyses

Approximately 25 adult fly thoraces were collected and homogenized in HBS buffer (210 mM mannitol, 70 mM sucrose, 5 mM HEPES [pH 7.4], 1 mM EGTA) containing protease inhibitor (Sigma). The lysate was centrifuged at 1,300 × *g* for 10 min, and the supernatant was collected and centrifuged again at 13,000 × *g* for 15 min. For coIP, the cytosolic and the mitochondrial fractions were incubated with anti-GFP- or anti-Myc-conjugated protein G agarose beads (Upstate) at 4°C for 2 hr. Beads were washed three times with PBS for 5 min each. Proteins were eluted and analyzed by western blot as described by Wu et al. (2013).

In Vitro Kinase and GTPase Assays

The conditions of the in vitro kinase assays were essentially as described by Lee et al. (2010). GST-Miro fusion protein production was carried out as described by Liu et al. (2012). In brief, cDNAs encoding fragments of dMiro were cloned into a glutathione S-transferase (GST)-encoding vector, pGEX-6P-1 (GE Healthcare), and GST fusion production was carried out in *Escherichia coli* strain *BL21*(*DE3*) cells according to the manufacturer's instructions. PLK1 and PKCζ were purchased from ProQinase. The GTPase assay for dMiro was performed according to a published procedure (Koshiba et al., 2011).

ATP Measurement

The level of ATP in *Drosophila* larval brain was measured essentially as previously described (Wu et al., 2013), using a luciferase-based bioluminescence assay kit (ATP Bioluminescence Assay Kit HS II; Roche Applied Science).

Calcium Imaging

For calcium imaging in primary neural cells, ~50 third-instar Tg larval brains expressing *Mito-GFP*, *Mito-GFP* + *UAS-dMiro-WT*, *Mito-GFP* + *UAS-dMiro-S66A*, or *Mito-GFP* + *dMiro RNAi* driven by *elav-GAL4* were collected. Primary neural cells were prepared according to published procedures (Egger et al., 2013). For monitoring of mitochondrial or cytosolic Ca^{2+} levels, primary neural cells were loaded with 1 μM Rhod-2 AM or Fluo-3 AM (Molecular Probes), respectively, in physiological salt solution (pH 7.4) (150 mM NaCl, 4 mM KCl, 1 mM $MgCl_2$, 5.6 mM glucose, 5 mM HEPES) for 30 min at 37°C. Primary neural cells were treated with 1 μM thapsigargin (Calbiochem) for intracellular Ca^{2+} perturbation. Calcium imaging was carried out using an inverted confocal microscope (LSM 510 META and LIVE 5; Carl Zeiss) with a 40× objective.

For measurement of mitochondrial Ca^{2+} in mammalian cells, HeLa cells were transfected with control *pCDNA3.0* vector or *Myc-hMiro1*, *Myc-hMiro2*, *Myc-dMiro-WT*, *Myc-dMiro-S66E*, or *Myc-dMiro-S66A* plasmids cloned in *pCDNA3.0*. After transfection, HeLa cells were loaded with Rhod-2 AM (10 μM in DMEM medium; Molecular Probes) for 30 min at room temperature. Cells were then washed with DMEM for 30 min. Single-cell fluorescence was excited at 545 nm and images of the emitted fluorescence obtained on a Leica TCS SP5 AOBS confocal microscope were processed with LAS AF (Leica).

Statistical Analysis

Statistical significance of all data was evaluated by two-tailed paired or unpaired Student's t tests. For studies employing multiple testing, we used one-way ANOVA followed by a Bonferroni post hoc test. All data are presented as mean ± SEM.

See Supplemental Experimental Procedures for additional details.

SUPPLEMENTAL INFORMATION

Supplemental Information includes Supplemental Experimental Procedures and seven figures and can be found with this article online at http://dx.doi.org/10.1016/j.devcel.2016.03.023.

AUTHOR CONTRIBUTIONS

S. Lee, K.-S.L., and S.H. designed the study, performed the experiments, analyzed data, wrote the manuscript, and contributed equally. S. Liu, D.-Y.L., and S.H.H. performed some of the experiments and contributed data. K.Y. participated in the supervision of the study and provided key reagents. B.L. conceived and supervised the study and wrote the manuscript.

ACKNOWLEDGMENTS

We are grateful to Drs. K. Zinsmaier, D.M. Glover, J. Lipsick, W.M. Saxton, D. Smith, J.K. Chung, I. Bezprozvanny, F. Kawasaki, A. Whitworth, Y.N. Jan, L. Luo, M. Guo, D. Walker, S. Davies, G. Hasan, J. Nambu, and the VDRC and Bloomington Stock Center for fly stocks and reagents. We thank members of the Lu laboratory for discussions and help. Supported by the NIH (R01NS083417 and R01MH080378 to B.L.), NRF (2014M3A908034462 to K.L. and 2015R1D1A1A01059079 to S.L.), and the Brainpool program of KOFST (to S.L.). B.L. is a founder and a member of the Scientific Advisory Board of NxGen Medicine, Inc. and PD Therapeutics, Inc.

Received: June 27, 2015
Revised: March 11, 2016
Accepted: March 23, 2016
Published: April 18, 2016

REFERENCES

Babic, M., Russo, G.J., Wellington, A.J., Sangston, R.M., Gonzalez, M., and Zinsmaier, K.E. (2015). Miro's N-Terminal GTPase domain is required for transport of mitochondria into axons and dendrites. J. Neurosci. *35*, 5754–5771.

Bahadorani, S., Cho, J., Lo, T., Contreras, H., Lawal, H.O., Krantz, D.E., Bradley, T.J., and Walker, D.W. (2010). Neuronal expression of a single-subunit yeast NADH-ubiquinone oxidoreductase (Ndi1) extends *Drosophila* lifespan. Aging Cell *9*, 191–202.

Bayraktar, O.A., and Doe, C.Q. (2013). Combinatorial temporal patterning in progenitors expands neural diversity. Nature *498*, 449–455.

Bello, B., Reichert, H., and Hirth, F. (2006). The brain tumor gene negatively regulates neural progenitor cell proliferation in the larval central brain of *Drosophila*. Development *133*, 2639–2648.

Boone, J.Q., and Doe, C.Q. (2008). Identification of *Drosophila* type II neuroblast lineages containing transit amplifying ganglion mother cells. Dev. Neurobiol. *68*, 1185–1195.

Bowman, S.K., Rolland, V., Betschinger, J., Kinsey, K.A., Emery, G., and Knoblich, J.A. (2008). The tumor suppressors Brat and Numb regulate transit-amplifying neuroblast lineages in *Drosophila*. Dev. Cell *14*, 535–546.

Brickley, K., Smith, M.J., Beck, M., and Stephenson, F.A. (2005). GRIF-1 and OIP106, members of a novel gene family of coiled-coil domain proteins: association in vivo and in vitro with kinesin. J. Biol. Chem. *280*, 14723–14732.

Cardenas, C., Miller, R.A., Smith, I., Bui, T., Molgo, J., Muller, M., Vais, H., Cheung, K.H., Yang, J., Parker, I., et al. (2010). Essential regulation of cell bioenergetics by constitutive InsP3 receptor Ca^{2+} transfer to mitochondria. Cell *142*, 270–283.

Castegna, A., Iacobazzi, V., and Infantino, V. (2015). The mitochondrial side of epigenetics. Physiol. Genomic. *47*, 299–307.

Chan, D.C. (2006). Mitochondria: dynamic organelles in disease, aging, and development. Cell *125*, 1241–1252.

Craig, S.N., Wyatt, M.D., and McInnes, C. (2014). Current assessment of polo-like kinases as anti-tumor drug targets. Expert Opin. Drug Disc. *9*, 773–789.

de Brito, O.M., and Scorrano, L. (2008). Mitofusin 2 tethers endoplasmic reticulum to mitochondria. Nature *456*, 605–610.

Dube, K.A., McDonald, D.G., and O'Donnell, M.J. (2000). Calcium homeostasis in larval and adult *Drosophila melanogaster*. Arch. Insect Biochem. Physiol. *44*, 27–39.

Egger, B., van Giesen, L., Moraru, M., and Sprecher, S.G. (2013). In vitro imaging of primary neural cell culture from *Drosophila*. Nat. Protoc. *8*, 958–965.

Fang, Y., Soares, L., Teng, X., Geary, M., and Bonini, N.M. (2012). A novel *Drosophila* model of nerve injury reveals an essential role of Nmnat in maintaining axonal integrity. Curr. Biol. *22*, 590–595.

Foley, K., and Cooley, L. (1998). Apoptosis in late stage *Drosophila* nurse cells does not require genes within the H99 deficiency. Development *125*, 1075–1082.

Fransson, A., Ruusala, A., and Aspenstrom, P. (2003). Atypical Rho GTPases have roles in mitochondrial homeostasis and apoptosis. J. Biol. Chem. *278*, 6495–6502.

Fransson, S., Ruusala, A., and Aspenstrom, P. (2006). The atypical Rho GTPases Miro-1 and Miro-2 have essential roles in mitochondrial trafficking. Biochem. Biophys. Res. Commun. *344*, 500–510.

Garcia-Rivas Gde, J., Carvajal, K., Correa, F., and Zazueta, C. (2006). Ru360, a specific mitochondrial calcium uptake inhibitor, improves cardiac post-ischaemic functional recovery in rats in vivo. Br. J. Pharmacol. *149*, 829–837.

Giorgi, C., Missiroli, S., Patergnani, S., Duszynski, J., Wieckowski, M.R., and Pinton, P. (2015). Mitochondria-associated membranes: composition, molecular mechanisms, and physiopathological implications. Antioxid. Redox Signal. *22*, 995–1019.

Glater, E.E., Megeath, L.J., Stowers, R.S., and Schwarz, T.L. (2006). Axonal transport of mitochondria requires Milton to recruit kinesin heavy chain and is light chain independent. J. Cell Biol. *173*, 545–557.

Guo, X., Macleod, G.T., Wellington, A., Hu, F., Panchumarthi, S., Schoenfield, M., Marin, L., Charlton, M.P., Atwood, H.L., and Zinsmaier, K.E. (2005). The GTPase dMiro is required for axonal transport of mitochondria to *Drosophila* synapses. Neuron *47*, 379–393.

Hajnoczky, G., Csordas, G., and Yi, M. (2002). Old players in a new role: mitochondria-associated membranes, VDAC, and ryanodine receptors as contributors to calcium signal propagation from endoplasmic reticulum to the mitochondria. Cell Calcium *32*, 363–377.

Hardie, D.G. (2007). AMP-activated/SNF1 protein kinases: conserved guardians of cellular energy. Nat. Rev. Mol. Cell Biol. *8*, 774–785.

Hayashi, T., Rizzuto, R., Hajnoczky, G., and Su, T.P. (2009). MAM: more than just a housekeeper. Trend Cell Biol. *19*, 81–88.

Hirokawa, N. (1998). Kinesin and dynein superfamily proteins and the mechanism of organelle transport. Science *279*, 519–526.

Howard, J. (1984). Calcium enables photoreceptor pigment migration in a mutant fly. J. Exp. Biol. *113*, 471–475.

Iijima-Ando, K., Hearn, S.A., Shenton, C., Gatt, A., Zhao, L., and Iijima, K. (2009). Mitochondrial mislocalization underlies Abeta42-induced neuronal dysfunction in a *Drosophila* model of Alzheimer's disease. PLoS One *4*, e8310.

Jouaville, L.S., Pinton, P., Bastianutto, C., Rutter, G.A., and Rizzuto, R. (1999). Regulation of mitochondrial ATP synthesis by calcium: evidence for a long-term metabolic priming. Proc. Natl. Acad. Sci. USA *96*, 13807–13812.

Kasahara, A., Cipolat, S., Chen, Y., Dorn, G.W., 2nd, and Scorrano, L. (2013). Mitochondrial fusion directs cardiomyocyte differentiation via calcineurin and Notch signaling. Science *342*, 734–737.

Kornmann, B., Osman, C., and Walter, P. (2011). The conserved GTPase Gem1 regulates endoplasmic reticulum-mitochondria connections. Proc. Natl. Acad. Sci. USA *108*, 14151–14156.

Koshiba, T., Holman, H.A., Kubara, K., Yasukawa, K., Kawabata, S., Okamoto, K., MacFarlane, J., and Shaw, J.M. (2011). Structure-function analysis of the yeast mitochondrial Rho GTPase, Gem1p: implications for mitochondrial inheritance. J. Biol. Chem. *286*, 354–362.

Lee, K.S., and Lu, B. (2014). The myriad roles of Miro in the nervous system: axonal transport of mitochondria and beyond. Front. Cell Neurosci. *8*, 330.

Lee, T., and Luo, L. (2001). Mosaic analysis with a repressible cell marker (MARCM) for *Drosophila* neural development. Trends Neurosci. *24*, 251–254.

Lee, S., Liu, H.P., Lin, W.Y., Guo, H., and Lu, B. (2010). LRRK2 kinase regulates synaptic morphology through distinct substrates at the presynaptic and postsynaptic compartments of the *Drosophila* neuromuscular junction. J. Neurosci. *30*, 16959–16969.

Lee, K.S., Wu, Z., Song, Y., Mitra, S.S., Feroze, A.H., Cheshier, S.H., and Lu, B. (2013). Roles of PINK1, mTORC2, and mitochondria in preserving brain tumor-forming stem cells in a noncanonical Notch signaling pathway. Genes Dev. *27*, 2642–2647.

Liu, S., Sawada, T., Lee, S., Yu, W., Silverio, G., Alapatt, P., Millan, I., Shen, A., Saxton, W., Kanao, T., et al. (2012). Parkinson's disease-associated kinase PINK1 regulates Miro protein level and axonal transport of mitochondria. PLoS Genet. *8*, e1002537.

Lutas, A., Wahlmark, C.J., Acharjee, S., and Kawasaki, F. (2012). Genetic analysis in *Drosophila* reveals a role for the mitochondrial protein p32 in synaptic transmission. G3 (Bethesda) *2*, 59–69.

Macaskill, A.F., Rinholm, J.E., Twelvetrees, A.E., Arancibia-Carcamo, I.L., Muir, J., Fransson, A., Aspenstrom, P., Attwell, D., and Kittler, J.T. (2009). Miro1 is a calcium sensor for glutamate receptor-dependent localization of mitochondria at synapses. Neuron *61*, 541–555.

MacAskill, A.F., Atkin, T.A., and Kittler, J.T. (2010). Mitochondrial trafficking and the provision of energy and calcium buffering at excitatory synapses. Eur. J. Neurosci. *32*, 231–240.

Malhotra, J.D., and Kaufman, R.J. (2011). ER stress and its functional link to mitochondria: role in cell survival and death. Cold Spring Harb. Perspect. Biol. *3*, a004424.

Manders, E.M.M., Verbeek, F.J., and Aten, J.A. (1993). Measurement of colocalization of objects in dual-color confocal images. J. Microsc. *169*, 375–382.

Mbefo, M.K., Paleologou, K.E., Boucharaba, A., Oueslati, A., Schell, H., Fournier, M., Olschewski, D., Yin, G., Zweckstetter, M., Masliah, E., et al. (2010). Phosphorylation of synucleins by members of the Polo-like kinase family. J. Biol. Chem. *285*, 2807–2822.

McCormack, J.G., Halestrap, A.P., and Denton, R.M. (1990). Role of calcium ions in regulation of mammalian intramitochondrial metabolism. Physiol. Rev. *70*, 391–425.

Messina, A., Neri, M., Perosa, F., Caggese, C., Marino, M., Caizzi, R., and De Pinto, V. (1996). Cloning and chromosomal localization of a cDNA encoding a mitochondrial porin from *Drosophila melanogaster*. FEBS Lett. *384*, 9–13.

Mitra, K., Rikhy, R., Lilly, M., and Lippincott-Schwartz, J. (2012). DRP1-dependent mitochondrial fission initiates follicle cell differentiation during *Drosophila* oogenesis. J. Cell Biol. *197*, 487–497.

Murley, A., Lackner, L.L., Osman, C., West, M., Voeltz, G.K., Walter, P., and Nunnari, J. (2013). ER-associated mitochondrial division links the distribution of mitochondria and mitochondrial DNA in yeast. ELife *2*, e00422.

Nguyen, T.T., Oh, S.S., Weaver, D., Lewandowska, A., Maxfield, D., Schuler, M.H., Smith, N.K., Macfarlane, J., Saunders, G., Palmer, C.A., et al. (2014). Loss of Miro1-directed mitochondrial movement results in a novel murine model for neuron disease. Proc. Natl. Acad. Sci. USA *111*, E3631–E3640.

Ouyang, Y., Petritsch, C., Wen, H., Jan, L., Jan, Y.N., and Lu, B. (2011). Dronc caspase exerts a non-apoptotic function to restrain phospho-Numb-induced ectopic neuroblast formation in *Drosophila*. Development *138*, 2185–2196.

Perocchi, F., Gohil, V.M., Girgis, H.S., Bao, X.R., McCombs, J.E., Palmer, A.E., and Mootha, V.K. (2010). MICU1 encodes a mitochondrial EF hand protein required for Ca(2+) uptake. Nature *467*, 291–296.

Pilling, A.D., Horiuchi, D., Lively, C.M., and Saxton, W.M. (2006). Kinesin-1 and Dynein are the primary motors for fast transport of mitochondria in *Drosophila* motor axons. Mol. Biol. Cell *17*, 2057–2068.

Rizzuto, R., Brini, M., Murgia, M., and Pozzan, T. (1993). Microdomains with high Ca^{2+} close to IP3-sensitive channels that are sensed by neighboring mitochondria. Science *262*, 744–747.

Rizzuto, R., Pinton, P., Carrington, W., Fay, F.S., Fogarty, K.E., Lifshitz, L.M., Tuft, R.A., and Pozzan, T. (1998). Close contacts with the endoplasmic reticulum as determinants of mitochondrial Ca^{2+} responses. Science *280*, 1763–1766.

Rizzuto, R., De Stefani, D., Raffaello, A., and Mammucari, C. (2012). Mitochondria as sensors and regulators of calcium signalling. Nat. Rev. Mol. Cell Biol. *13*, 566–578.

Rowland, A.A., and Voeltz, G.K. (2012). Endoplasmic reticulum-mitochondria contacts: function of the junction. Nat. Rev. Mol. Cell Biol. *13*, 607–625.

Rozeboom, A.M., and Pak, D.T. (2012). Identification and functional characterization of polo-like kinase 2 autoregulatory sites. Neuroscience *202*, 147–157.

Sanz, A., Soikkeli, M., Portero-Otin, M., Wilson, A., Kemppainen, E., McIlroy, G., Ellila, S., Kemppainen, K.K., Tuomela, T., Lakanmaa, M., et al. (2010). Expression of the yeast NADH dehydrogenase Ndi1 in *Drosophila* confers increased lifespan independently of dietary restriction. Proc. Natl. Acad. Sci. USA *107*, 9105–9110.

Saotome, M., Safiulina, D., Szabadkai, G., Das, S., Fransson, A., Aspenstrom, P., Rizzuto, R., and Hajnoczky, G. (2008). Bidirectional Ca^{2+}-dependent control of mitochondrial dynamics by the Miro GTPase. Proc. Natl. Acad. Sci. USA *105*, 20728–20733.

Schon, E.A., and Area-Gomez, E. (2013). Mitochondria-associated ER membranes in Alzheimer disease. Mol. Cell Neurosci. *55*, 26–36.

Schon, E.A., and Przedborski, S. (2011). Mitochondria: the next (neurode)generation. Neuron *70*, 1033–1053.

Sheng, Z.H., and Cai, Q. (2012). Mitochondrial transport in neurons: impact on synaptic homeostasis and neurodegeneration. Nat. Rev. Neurosci. *13*, 77–93.

Shim, J., Mukherjee, T., Mondal, B.C., Liu, T., Young, G.C., Wijewarnasuriya, D.P., and Banerjee, U. (2013). Olfactory control of blood progenitor maintenance. Cell *155*, 1141–1153.

Song, Y., and Lu, B. (2011). Regulation of cell growth by Notch signaling and its differential requirement in normal vs. tumor-forming stem cells in *Drosophila*. Genes Dev. *25*, 2644–2658.

Stowers, R.S., Megeath, L.J., Gorska-Andrzejak, J., Meinertzhagen, I.A., and Schwarz, T.L. (2002). Axonal transport of mitochondria to synapses depends on Milton, a novel *Drosophila* protein. Neuron *36*, 1063–1077.

Tait, S.W., and Green, D.R. (2012). Mitochondria and cell signalling. J. Cell Sci. *125*, 807–815.

Tang, T.S., Slow, E., Lupu, V., Stavrovskaya, I.G., Sugimori, M., Llinas, R., Kristal, B.S., Hayden, M.R., and Bezprozvanny, I. (2005). Disturbed Ca^{2+} signaling and apoptosis of medium spiny neurons in Huntington's disease. Proc. Natl. Acad. Sci. USA *102*, 2602–2607.

Teixeira, F.K., Sanchez, C.G., Hurd, T.R., Seifert, J.R., Czech, B., Preall, J.B., Hannon, G.J., and Lehmann, R. (2015). ATP synthase promotes germ cell differentiation independent of oxidative phosphorylation. Nat. Cell Biol. *17*, 689–696.

Terhzaz, S., Southall, T.D., Lilley, K.S., Kean, L., Allan, A.K., Davies, S.A., and Dow, J.A. (2006). Differential gel electrophoresis and transgenic mitochondrial calcium reporters demonstrate spatiotemporal filtering in calcium control of mitochondria. J. Biol. Chem. *281*, 18849–18858.

Tu, H., Nelson, O., Bezprozvanny, A., Wang, Z., Lee, S.F., Hao, Y.H., Serneels, L., De Strooper, B., Yu, G., and Bezprozvanny, I. (2006). Presenilins form ER Ca^{2+} leak channels, a function disrupted by familial Alzheimer's disease-linked mutations. Cell *126*, 981–993.

Venkatesh, K., and Hasan, G. (1997). Disruption of the IP3 receptor gene of *Drosophila* affects larval metamorphosis and ecdysone release. Curr. Biol. *7*, 500–509.

Vos, M., Lauwers, E., and Verstreken, P. (2010). Synaptic mitochondria in synaptic transmission and organization of vesicle pools in health and disease. Front. Synaptic Neurosci. *2*, 139.

Wallace, D.C. (2005). A mitochondrial paradigm of metabolic and degenerative diseases, aging, and cancer: a dawn for evolutionary medicine. Annu. Rev. Genet. *39*, 359–407.

Wallace, D.C. (2010). The epigenome and the mitochondrion: bioenergetics and the environment [corrected]. Genes Dev. *24*, 1571–1573.

Wang, X., and Schwarz, T.L. (2009). The mechanism of Ca^{2+}-dependent regulation of kinesin-mediated mitochondrial motility. Cell *136*, 163–174.

Wang, H., Ouyang, Y., Somers, W.G., Chia, W., and Lu, B. (2007). Polo inhibits progenitor self-renewal and regulates Numb asymmetry by phosphorylating Pon. Nature *449*, 96–100.

Wang, X., Winter, D., Ashrafi, G., Schlehe, J., Wong, Y.L., Selkoe, D., Rice, S., Steen, J., Lavoie, M.J., and Schwarz, T.L. (2011). PINK1 and Parkin target Miro for phosphorylation and degradation to arrest mitochondrial motility. Cell *147*, 893–906.

Wu, Z., Sawada, T., Shiba, K., Liu, S., Kanao, T., Takahashi, R., Hattori, N., Imai, Y., and Lu, B. (2013). Tricornered/NDR kinase signaling mediates PINK1-directed mitochondrial quality control and tissue maintenance. Genes Dev. *27*, 157–162.